J. Math. Biol. (2010) 60:75–94
DOI 10.1007/s00285-009-0259-6

Mathematical Biology

# Numerical simulation of blood and interstitial flow through a solid tumor

**C. Pozrikidis**

Received: 28 August 2008 / Revised: 22 December 2008 / Published online: 11 March 2009


**Abstract** A theoretical framework is presented for describing blood flow through the irregular vasculature of a solid tumor. The tumor capillary bed is modeled as a capillary tree of bifurcating segments whose geometrical construction involves deterministic and random parameters. Blood flow along the individual capillaries accounts for plasma leakage through the capillary walls due to the transmural pressure according to Sterling's law. The extravasation flow into the interstitium is described by Darcy's law for a biological porous medium. The pressure field developing in the interstitium is computed by solving Laplace's equation subject to derived boundary conditions at the capillary vessel walls. Given the arterial, venous, and tumor surface pressures, the problem is formulated as a coupled system of integral and differential equations arising from the interstitium and capillary flow transport equations. Numerical discretization yields a system of linear algebraic equations for the interstitial and capillary segment pressures whose solution is found by iterative methods. Results of numerical computations document the effect of the interstitial hydraulic and vascular permeability on the fractional plasma leakage. Given the material properties, the fractional leakage reaches a maximum at a particular grade of the bifurcating vascular tree.

**Keywords** Solid tumor · Blood flow · Numerical methods · Integral equations

**Mathematics Subject Classification (2000)** 92C10 · 92B99 · 45B05

C. Pozrikidis (✉)
Department of Chemical Engineering, University of Massachusetts,
Amherst, MA 01003, USA
e-mail: cpozrikidis@ecs.umass.edu

## 1 Introduction

The capillary bed of normal tissue exhibits a high degree of geometrical regularity that helps minimize the resistance to blood flow and promotes the uniform transport of oxygen, nutrients, and metabolites. In contrast, the neoplastic vasculature of a solid tumor is dilated and strikingly disorganized, to the extent that it is often difficult to distinguish between venules and arterioles. Tortuous vessels, curved and spiral loops, shunts, avascular and poorly vascularized regions, and low vascular density contribute to the complexity of the malignant microstructure. The process of tumor angiogenesis has received considerable attention in the medical and engineering literature. Elementary and advanced mathematical models of tumor growth and blood vessel proliferation driven by chemotaxis are available (e.g., Chaplain et al. 2006).

Less et al. (1991) studied the microvascular architecture of the mammary adenocarcinoma and found that the arterial network consists of vessels with mean segment length $L_c \sim 67\mu$m, mean radius $a_c \sim 5\mu$m, and minimum distance between any two non-adjacent pairs of capillary segments (inter-capillary distance) 49 μm. The venous vasculature consists of capillary vessels whose diameter ranges from 20 to 650 μm. Due to its pronounced randomness, the vascular architecture can be characterized using diagnostics of fractal geometry. Studies have shown that the fractal dimension of the tumor vasculature is intermediate between that of the normal arterial tree and of the subcateneous capillary network (e.g., Baish and Jain 2000; Chung and Chung 2001; Gazit and Baish 1997). Because of the highly irregular geometrical microstructure, reduced oxygen concentration, and altered chemical environment, blood flow through the neoplastic vasculature significantly differs from that through a healthy capillary bed. Some tumor vessels do not carry red blood cells and are thus deficient in oxygen and nutrients. Other vessels, including shunt vessels with large diameter, carry an abundance of red blood cells. Low oxygen concentration causes red blood cell stiffening and agglomeration, and this increases the effective viscosity of blood and may effectively stop the flow.

Investigations of flow through the neoplastic vasculature and interstitium of solid tumors has been motivated by the urgent need to understand and improve the role of fluid convection in the treatment of cancer by therapeutic macromolecules. In drug therapy, monoclonal antibodies (MAbs) are delivered intravenously in the hope that they will reach the tumor cancer cells as they travel through the circulation. The macromolecules are transported by convection along the capillaries and by convection and diffusion into the tumor interstitium. The success of this treatment has been limited because of low transport rates into the main body of the tumor across the vasculature, and also because of the small diffusivity of the therapeutic macromolecules (Vaughan et al. 1987). External beam radiation, hyperthermia, and deliberate inflammation have been attempted to overcome these limitations, albeit with moderate only success. Convection induced by elevating the systemic blood pressure or by intratumoral infusion has been shown to improve drug delivery, respectively, by 40% and by several orders of magnitude (Zhang et al. 2000). Similar difficulties are encountered in the case of immunotherapy where altered white blood cells migrate across the tumor vasculature to destroy specifically targeted malignant cells. A considerable body of clinical, laboratory, and theoretical investigations have been conducted on the realization that an

improvement in the efficiency of drug therapy can be achieved only if a fundamental understanding of the processes by which the macromolecules reach the tumor cancer cells is gained (Dreher et al. 2006).

Efforts have been made to describe fluid flow and species transport in solid tumors by macroscopic theoretical analysis and phenomenological descriptions. Jain and coworkers (Jain and Baxter 1988; Baxter and Jain 1989, 1990) developed a model consisting of a spherical tumor with a necrotic concentric core and a continuously distributed vasculature in the presence of lymphatics. The pressure distribution in the interstitium was described by Helmholtz's equation derived from Darcy's law under the assumption that the net flow into the interstitium is balanced by the efflux from the vasculature due to convection and the influx into the lymphatics. The transport of macromolecules was described by a convection–diffusion equation accounting for the capillary exchange. El-Kareh and Secomb (1995) adopted this model to study the effect of tumor shape, and concluded that increasing the vascular permeability does not always improve the convective transport of antibodies.

Other authors recognized the importance of describing fluid flow and species transport on the level of the capillaries, and developed models that explicitly take into consideration the geometry of the vascular microstructure. Netti et al. (1996) modeled the tumor vasculature as an equivalent permeable vessel embedded in a uniform-pressure medium, and carried out simulations to study the effect of vessel leakiness, vessel compliance, and interstitial fluid pressure on the pressure-flow relationship, arterial-venous pressure relationship, and pressure profile along the vessel. Baish et al. (1997) described the fluid flow through the microcirculatory network and interstitium using a network model that consists of a regular mesh of permeable vessels or a pair of counter-current vessels embedded in an isotropic porous medium. Milosevic et al. (1999) modified the single-capillary model of Netti et al. (1996) by computing the interstitial fluid pressure on the outer surface of the capillary based on a global mass balance applied to an idealized spherical tumor encapsulating the capillary. More recently, Pozrikidis and Farrow (2003) developed an integrated model that couples blood flow through the capillaries, the extravasation flux, and the flow in the interstitium, and performed computations for a simple model consisting of a single capillary to demonstrate the feasibility of this approach.

The present paper extends the single-tube model of Pozrikidis and Farrow (2003) into a network model, where the vasculature is represented by a branching tree consisting of a cascade of straight bifurcating capillary segments. The geometrical construction involves deterministic and random parameters causing deviations from a perfectly ordered structure. Fluid escapes from the capillary walls according to the local transmural pressure generating an extravasation flow in the interstitium according to Darcy's law. The problem is formulated as a coupled system of integral and differential equations, subject to a specified arterial, venous, and tumor exterior surface pressures. Numerical discretization in the spirit of the boundary-element method yields systems of linear algebraic equations for the interstitial and capillary segment pressures whose solution is found by iteration. Results of numerical computations illustrate the structure of the vascular and interstitial pressure fields and document the effect of the interstitial hydraulic and vascular permeability on the fractional leakage associated with perfusion. Extensions and refinements of the basic model and

consideration of different vascular geometries are possible, as discussed in the concluding section.

## 2 Theoretical model

We consider blood flow through a model capillary network embedded in tumor tissue, as shown in Fig. 1a. The arterial entrance point coincides with the first end-point of the first capillary segment in the $xy$ plane with specified length $L_{c_1}$ and radius $a_{c_1}$. A sequence of bifurcations is then introduced to produce a branching network resembling a fractal tree. The length of the projection of each capillary segment in the $xy$ plane is $L_c = \omega\, L'_c\,[1 + \epsilon_L(r - 0.5)]$, where $L'_c$ is the length of the parent segment, $\omega$ is a specified contraction ratio, $\epsilon_L$ is a specified dimensionless parameter, and $r$ is a uniform deviate. The bifurcation angle in the $xy$ plane is $\theta = \pm\theta_0 + \epsilon_\theta(r - 0.5)\pi$, where $\theta_0$ is a specified mean semi-angle, $\epsilon_\theta$ is a specified dimensionless parameter, and $r$ is another uniform deviate.

After a capillary bifurcation has been generated parallel to the $xy$ plane, the second end point of each newly created capillary segment is displaced normal to the $xy$ plane by the positive or negative distance $z = L_{c_1}\,\epsilon_z(r - 0.5)$, where $\epsilon_z$ is another specified dimensionless parameters. The radius of each generated capillary segment is reduced geometrically with respect to that of the parent segment, so that the last bifurcation yields a specified minimum radius, $a_{c_{\min}}$. The geometrical construction is consistent with the flattened annular-shell shape of the tumor vasculature surrounding a necrotic core (e.g., Tsafnat et al. 2004). A similar construction was used by Karshafian et al. (2003) in their study of blood flow through a fractal-like vascular network.

Figure 1b schematically illustrates flow through the vascular network of a solid tumor originating from an arterial entrance point. Because the walls of the blood vessels are permeable, plasma escapes by convection into the interstitium and is either removed by lymphatic vessels or exits into the surrounding tissue across the tumor surface, as indicated by the arrows. The arterial vascular network is connected to an attached venous network, drawn with the dashed lines in Fig. 1b. Since the pressure drop across the venules is small, the venous pressure is assumed to be constant at the terminal branches of the bifurcating tree, and the flow rate is computed as part of the solution.

We set up the theoretical model by regarding the interstitium as an isotropic and homogeneous biological porous material. Flow through the interstitium is described by Darcy's law relating the average fluid velocity, $\mathbf{u}$, to the gradient of the interstitial pressure, $p$,

$$\mathbf{u} = -\kappa\,\nabla p, \tag{2.1}$$

where $\kappa = \lambda/\mu_i$ is the hydraulic permeability, $\lambda$ is the interstitium permeability, and $\mu_i$ is the interstitium fluid viscosity. The dependence of $\kappa$ on the tumor tissue composition and environment has been discussed by Jain (1987). The hydraulic permeability of the dog squamous cell tissue was estimated to be on the order of $10^{-9}\,\text{cm}^4/(\text{dyn s})$, and the hydraulic conductivity of the Hepatoma 5,123 tissue was estimated to be on the

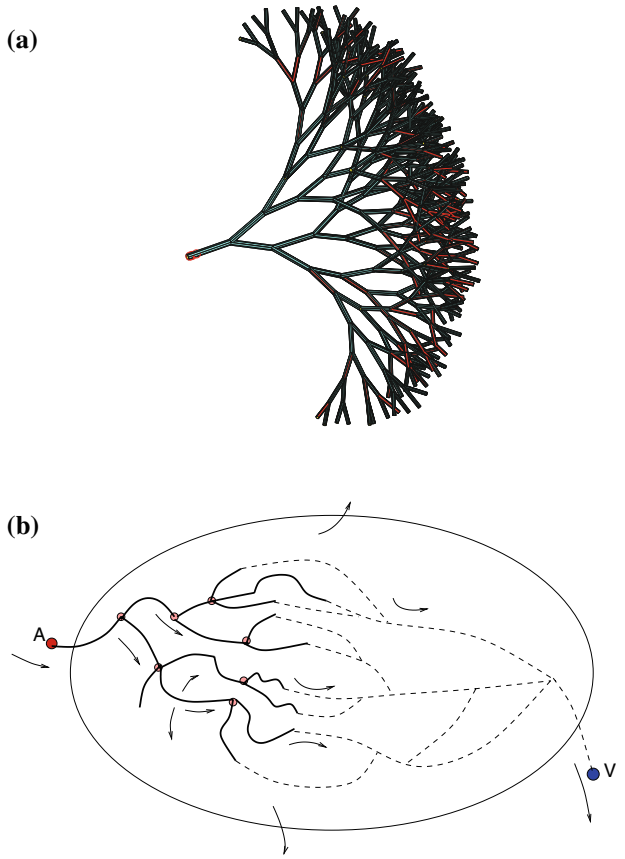


**Fig. 1** **a** A model tree-like capillary network exhibiting random bifurcations and terminating after a specified number of bifurcations. The capillary radius decreases geometrically by a constant factor from the arterial entrance point to the exit points of the smallest capillaries. **b** Schematic illustration of blood flow through the vasculature of a solid tumor originating from an arterial entrance point, $A$, and ending at a venous exit point, $V$. The solid lines trace arterial vessels, and the broken lines trace venous vessels

order of $10^{-12}$ cm$^4$/(dyn s). For comparison, we note that the hydraulic permeability of normal tissue varies in the range $10^{-12}$–$10^{-10}$ cm$^4$/(dyn s) (e.g., Fleischman et al. 1986a).

Mass conservation in the absence of consumption due to lymphatics requires that the average velocity field inside the tumor is solenoidal. Taking the divergence of Darcy's law expressed by (2.1) we find that the interstitial pressure satisfies Laplace's equation,

$$\nabla^2 p = 0. \tag{2.2}$$

The solution must satisfy a Dirichlet boundary condition stating that $p$ is equal to the ambient pressure at the tumor surface, denoted as $p_\infty$.

In the physiologically relevant range of pressure drops across the vascular network, the Reynolds number of the flow along the capillaries is much less than unity (Sevick and Jain 1989a,b). Assuming that the radius of the capillaries, $a$, is a sufficiently smooth function of distance along the centerline, $l$, and the rate of fluid transport through the vascular walls is small compared to the axial flow rate, we describe the axial flow rate through a capillary by Poiseuille's law,

$$Q_c = -\frac{\pi a^4(l)}{8\mu}\,\frac{\mathrm{d}p_c}{\mathrm{d}l}, \tag{2.3}$$

where $\mu$ is the blood viscosity and $p_c(l)$ is the position-dependent pressure inside the capillary. In the case of tumor capillary flow, the Poiseuille law should be regarded as an approximation, essentially implementing functional dependencies on the fluid viscosity and blood vessel radius. Improvements can be made to incorporate capillary wall curvature, waviness, and tapering.

Next, we describe the extravasation flux of plasma fluid across the vasculature into the surrounding interstitium by Starling's law

$$q_e(l) = L_p\,[p_c(l) - p(l)], \tag{2.4}$$

where $L_p$ is the vascular permeability of the tube wall. In Starling's law, the interstitial pressure, $p(l)$, is evaluated on the exterior side of the vascular wall and is assumed to be nearly independent of angular position around the centerline due to the small size of the capillaries (e.g., Fleischman et al. 1986a,b). It is known that the tumor vascular permeability is higher by a factor of ten than that in nonmalignant tissue due to the coarse and irregular structure of the neoplastic endothelium (e.g., Baish et al. 1997; Baxter and Jain 1989; Sands et al. 1988). Baish et al. (1997) provide the estimate $L_p \simeq 10^{-9}$ cm$^3$/(dyn s). Because of the high vascular permeability and lack of functional lymphatics, the concentration of plasma proteins is higher in tumor than in normal tissue (retention effect.) The accumulation of macromolecules injected by intravenous administration makes them desirable in tumor diagnosis and therapy as drug carriers (Dreher et al. 2006).

Mass conservation for the fluid transported along a capillary requires

$$\frac{\mathrm{d}Q_c}{\mathrm{d}l} + 2\pi a(l)\,q_e(l) = 0. \tag{2.5}$$

Substituting (2.3) and (2.4) in (2.5) and rearranging, we derive the second-order differential equation

$$\frac{\mathrm{d}^2 p_c}{\mathrm{d}l^2} + \frac{4}{a(l)}\,\frac{\mathrm{d}a}{\mathrm{d}l}\,\frac{\mathrm{d}p_c}{\mathrm{d}l} = \frac{16\mu L_p}{a^3(l)}\,[p_c(l) - p(l)]\,. \tag{2.6}$$

Only if $p(l)$ is constant the capillary flow is decoupled from the interstitial flow and can be solved in isolation. However, unlike in healthy tissue, the pressure inside a

solid tumor exhibit pronounced variation and a sharp decline across an outer annular shell.

To complete the mathematical formulation, we set the flux given by Darcy's law at the tube surface equal to that given by Starling's law to derive an expression for the normal derivative of the tumor pressure,

$$\frac{\partial p}{\partial l_n} \equiv \mathbf{n}(\mathbf{x}) \cdot \nabla p(\mathbf{x}) \simeq -\frac{q_e}{\kappa} = -\frac{L_p}{\kappa} [p_c(l) - p(l)], \tag{2.7}$$

where $\mathbf{n}$ is the unit vector normal to the vasculature pointing into the interstitium, and $l_n$ is the normal arc length.

A central task is the numerical solution of Laplace's equation (2.2) for the interstitial pressure, $p$, subject to boundary conditions at the tumor surface and over the exterior surface of the vasculature. The boundary-integral formulation provides us with an expression for the interstitial pressure at a field point, $\mathbf{x}_0$, in terms of combination of a single- and a double-layer potential defined over the surface of the vasculature, $S_V$,

$$\begin{aligned} p(\mathbf{x}_0) = p_\infty &- \iint_{S_V} G(\mathbf{x}, \mathbf{x}_0) \, [\mathbf{n}(\mathbf{x}) \cdot \nabla p(\mathbf{x})] \, \mathrm{d}S(\mathbf{x}) \\ &+ \iint_{S_V} (p(\mathbf{x}) - p_\infty) \, [\mathbf{n}(\mathbf{x}) \cdot \nabla G(\mathbf{x}, \mathbf{x}_0)] \, \mathrm{d}S(\mathbf{x}), \end{aligned} \tag{2.8}$$

where $G(\mathbf{x}, \mathbf{x}_0)$ is the Green's function of Laplace's equation corresponding to the tumor shape. The difference $p(\mathbf{x}) - p_\infty$ expresses the disturbance pressure field due to extravasation. By definition, $G(\mathbf{x}, \mathbf{x}_0) = 0$ when either $\mathbf{x}$ or $\mathbf{x}_0$ lies at the tumor surface (e.g., Pozrikidis 1997). In the case of a large, virtually infinite tumor, $G(\mathbf{x}, \mathbf{x}_0) = 1/(4\pi|\mathbf{x} - \mathbf{x}_0|)$ is the free-space Green's function. Substituting the boundary condition (2.7) in the first integral on the right-hand side of (2.8) and invoking our earlier approximation that the interstitial pressure is nearly independent of angular position around the capillaries, we obtain

$$\begin{aligned} p(\mathbf{x}_0) = p_\infty &+ \frac{1}{\kappa} \iint_{S_V} L_p \, [p_c(l) - p(l)] \, G(\mathbf{x}, \mathbf{x}_0) \, \mathrm{d}S(\mathbf{x}) \\ &+ \iint_{S_V} (p(l) - p_\infty) \, [\mathbf{n}(\mathbf{x}) \cdot \nabla G(\mathbf{x}, \mathbf{x}_0)] \, \mathrm{d}S(\mathbf{x}), \end{aligned} \tag{2.9}$$

which provides us with a representation of the interstitial pressure in terms of the vascular distribution of the interstitium and capillary pressures.

Next, we take the limit as the point $\mathbf{x}_0$ approaches the surface of the vasculature from the outside. The limit of the double-layer potential differs from the value of the double-layer potential computed when the point $\mathbf{x}_0$ lies precisely on the vasculature, termed the principal value. Expressing the limit in terms of its principal value, denoted

by $PV$, we derive the integral equation

$$\frac{1}{2}\,(p(\mathbf{x}_0)-p_\infty) = \frac{1}{\kappa}\iint\limits_{S_V} L_p\,[p_c(l)-p(l)]\,G(\mathbf{x},\mathbf{x}_0)\,\mathrm{d}S(\mathbf{x}) + \iint\limits_{S_V}^{PV} (p(l)-p_\infty)\;[\mathbf{n}(\mathbf{x})\cdot\nabla G(\mathbf{x},\mathbf{x}_0)]\;\mathrm{d}S(\mathbf{x}). \tag{2.10}$$

The problem has been reduced to simultaneously solving the differential equation (2.6) and the integral equation (2.10), subject to specified values for the arterial inlet pressure $p_a$, venous outlet pressure, $p_v$, and tumor surface pressure, $p_\infty$.

## 3 Numerical method

The interstitial and vascular pressures are now approximated with constant functions over the $j$th capillary segment denoted, respectively, by $p^{(j)}$ and $p_c^{(j)}$, for $j = 1,\ldots,N_s$, where $N_s$ is the total number of segments. Subject to this approximation, the integral equation (2.10) takes the form

$$\frac{1}{2}\,(p(l_0)-p_\infty) = \frac{L_p}{\kappa}\sum_{j=1}^{N_s}(p_c^{(j)}-p^{(j)})\,A_j(l_0) + \sum_{j=1}^{N_s}(p^{(j)}-p_\infty)\,B_j(l_0), \tag{3.1}$$

where

$$A_j(l_0) \equiv \iint\limits_{E_j} G(\mathbf{x},\mathbf{x}_0)\,\mathrm{d}S(\mathbf{x}), \quad B_j(l_0) \equiv \iint\limits_{E_j}^{PV} \mathbf{n}(\mathbf{x})\cdot\nabla G(\mathbf{x},\mathbf{x}_0)\,\mathrm{d}S(\mathbf{x}), \tag{3.2}$$

are influence coefficients for the single-layer and double-layer potential, and $E_j$ denotes the cylindrical surface of the $j$th segment.

Placing the evaluation point corresponding to arc-length, $l_0$, at the mid-point of the $n$th segment corresponding to arc length $l_n^m$, we derive a system

$$\frac{1}{2}(p^{(n)}-p_\infty) = \frac{L_p}{\kappa}\sum_{j=1}^{N_s}(p_c^{(j)}-p^{(j)})A_j(l_n^m) + \sum_{i=1}^{N_s}(p^{(j)}-p_\infty)\,B_j(l_n^m), \tag{3.3}$$

where $n = 1,\ldots,N_s$. Now transferring the interstitial pressures to the left-hand side and rearranging, we obtain

$$\sum_{j=1}^{N_s}\left[\frac{1}{2}\,\delta_{nj} - B_j(l_n^m) + \frac{L_p}{\kappa}\,A_j(l_n^m)\right] p^{(j)} = \frac{L_p}{\kappa}\sum_{j=1}^{N_s} p_c^{(j)}A_j(l_n^m) + p_\infty\left[\frac{1}{2} - \sum_{j=1}^{N_s} B_j(l_n^m)\right], \tag{3.4}$$

where $\delta_{nj}$ is Kronecker's delta. An integral identity states that the integral whose approximate representation is given by the second sum on the right-hand side of (3.4) is equal to $-\frac{1}{2}$. In the discrete formulation of the problem, this identity is satisfied up to the numerical error due to the spatial discretization and numerical integration. To ensure that, when $p_a = p_v = p_\infty$, the segment pressures arising from the solution of (3.4) are equal to $p_\infty$ to machine precision, we retain the second sum on the right-hand side.

The surface integrals in (3.2) are computed by first performing the integration with respect to the meridional angle around each cylindrical segment to obtain a one-dimensional integral along the generator involving complete elliptic integrals of the first and second kind, and then integrating with respect to distance along the segment axis using the six-point Gauss-Legendre quadrature (e.g., Pozrikidis 1997). The complete elliptical integrals are evaluated using an accurate iterative method (e.g., Pozrikidis 2008). When the evaluation point lies at the host segment, the influence coefficient of the single-layer potential, $A_j$, exhibits a logarithmic singularity. For improved accuracy, this singularity is subtracted off and then integrated analytically by elementary methods. The principal value of the influence coefficient of the double-layer potential, $B_j$, is computed using an integral identity that replaces the integral over the cylindrical surface of a segment with integrals over the disk-like segment ends.

### 3.1 Capillary flow

Next, we apply the capillary flow Eq. (2.6) for constant tube radius at the midpoint of the $j$th capillary segment to obtain

$$\frac{\mathrm{d}^2 p_c}{\mathrm{d}l^2} = \frac{16\mu L_p}{a^3}(p_c - p), \tag{3.5}$$

where the segment label $(j)$ has been omitted for clarity. Introducing segment end- and mid-point values indicated by the subscripts $-1, 0, 1$ and approximating the second derivative with a central difference, we find

$$\frac{p_1 - 2p_0 + p_{-1}}{\Delta l^2} = \frac{16\mu L_p}{a^3}(p_0 - p), \tag{3.6}$$

where $\Delta l = L_c/2$, and $L_c$ is the capillary segment length. Rearranging, we derive an expression for the midpoint value in terms of the end point values,

$$p_0 = \frac{p_1 + p_{-1} + \beta\, p}{2 + \beta}, \tag{3.7}$$

where

$$\beta = \frac{16\mu L_p \Delta l^2}{a^3} = \frac{4\mu L_p L_c^2}{a^3} \tag{3.8}$$

is a dimensionless parameter. Now using (3.7), we find the transmural pressure

$$p_0 - p = \frac{p_1 - 2p + p_{-1}}{2 + \beta}. \tag{3.9}$$

This expression is used to compute the extravasation flux in the discretized boundary integral formulation.

Using a second-order difference approximation, we compute the pressure gradient at the segment end nodes,

$$\left(\frac{\mathrm{d}p_c}{\mathrm{d}l}\right)_{-1} \simeq \frac{-3\,p_{-1} + 4\,p_0 - p_1}{2\Delta l}, \quad \left(\frac{\mathrm{d}p_c}{\mathrm{d}l}\right)_{1} \simeq \frac{p_{-1} - 4\,p_0 + 3\,p_1}{2\Delta l}. \tag{3.10}$$

Eliminating the mid-node pressure, $p_0$, using (3.7), we find

$$\begin{aligned} \left(\frac{\mathrm{d}p_c}{\mathrm{d}l}\right)_{-1} &\simeq \frac{-(3\beta + 2)\,p_{-1} + 4\beta\,p + (2 - \beta)\,p_1}{(2 + \beta)\,2\Delta l}, \\ \left(\frac{\mathrm{d}p_c}{\mathrm{d}l}\right)_{1} &\simeq \frac{-(2 - \beta)\,p_{-1} - 4\beta\,p + (3\beta + 2)\,p_1}{(2 + \beta)\,2\Delta l}. \end{aligned} \tag{3.11}$$

The flow rates at the two ends of the capillary segment are

$$\begin{aligned} Q_{-1} &= -\left(\frac{\mathrm{d}p_c}{\mathrm{d}l}\right)_{-1} \frac{\pi a^4}{8\mu} \simeq (c_A\,p_{-1} - c_C\,p - c_B\,p_1)\,\frac{\pi a^4}{8L_c\mu}, \\ Q_1 &= -\left(\frac{\mathrm{d}p_c}{\mathrm{d}l}\right)_{1} \frac{\pi a^4}{8\mu} \simeq (c_B\,p_{-1} + c_C\,p - c_A\,p_1)\,\frac{\pi a^4}{8L_c\mu}, \end{aligned} \tag{3.12}$$

where

$$c_B = \frac{2 - \beta}{2 + \beta}, \quad c_C = \frac{4\beta}{2 + \beta}, \quad c_A = \frac{2 + 3\beta}{2 + \beta}. \tag{3.13}$$

In the absence of extravasation, $\beta = 0$, we obtain the expected result, $c_B = 1, c_C = 0$, and $c_A = 1$. The rate of fluid extravasating through the capillary wall is

$$Q_e = Q_1 - Q_{-1} \simeq -[(c_A - c_B)\,p_{-1} - 2\,c_C\,p + (c_A - c_B)\,p_1]\,\frac{\pi a^4}{8L_c\mu}, \tag{3.14}$$

which is consistent with (3.9) and the definition of $\beta$.

To examine the error associated with the finite-difference approximation, we express the differential equation (3.5) in the form

$$\frac{\mathrm{d}^2 p_c}{\mathrm{d}\hat{x}^2} = 4\beta\,(p_c - p), \tag{3.15}$$

where $\hat{x} = l/L_c$. Next, we consider a capillary segment beginning at the arterial entrance point, $x = 0$, where $p_c = p_a$, and ending at the venous entrance point, $x = L_c$, where $p_v = 0$. For constant interstitial pressure, $p$, the solution for the capillary pressure distribution can be found readily by elementary analytical methods,

$$p_c(\hat{x}) = p_a[\cosh(2\sqrt{\beta}\hat{x}) - \sinh(2\sqrt{\beta}\hat{x})\coth(2\sqrt{\beta})\,] + p\left[1 - \frac{1-\cosh(2\sqrt{\beta})}{\sinh(2\sqrt{\beta})}\sinh(2\sqrt{\beta}\,\hat{x}) - \cosh(2\sqrt{\beta}\,\hat{x})\right]. \quad (3.16)$$

The midpoint value is $p_c(\hat{x} = 1/2) = p_a\,\Phi(\beta) + p\,\Xi(\beta)$, where

$$\Phi(\beta) = \cosh(\sqrt{\beta}) - \sinh(\sqrt{\beta})\coth(2\sqrt{\beta})\,],$$
$$\Xi(\beta) = 1 - \frac{1-\cosh(2\sqrt{\beta})}{\sinh(2\sqrt{\beta})}\sinh(\sqrt{\beta}) - \cosh(\sqrt{\beta}). \quad (3.17)$$

The finite-difference method predicts the approximate values $\Phi \simeq 1/(2+\beta)$ and $\Xi \simeq \beta/(2+\beta)$. The predictions are compared in Fig. 2a, b in a range of $\beta$ encompassing the physiological values considered in the numerical computations, as discussed in Sect. 4. For example, setting $\lambda = 4\,\mathrm{cp}$, $L_p = 10^{-6}\,\mathrm{cm}^3/(\mathrm{dyn\ s})$, $L_c = 0.01\,\mathrm{cm}$, and $a = 6\times10^{-4}\,\mathrm{cm}$, we find $\beta = 0.0741$. The comparison lends credence to the finite-difference approximation.

As a further test, we consider the end-point pressure gradients,

$$\left(\frac{\mathrm{d}p_c}{\mathrm{d}x}\right)_{\hat{x}=0} = -\frac{p_a}{L_c}\,\Psi_0 + \frac{p}{L_c}\,\Psi, \quad \left(\frac{\mathrm{d}p_c}{\mathrm{d}x}\right)_{\hat{x}=1} = -\frac{p_a}{L_c}\,\Psi_1 - \frac{p}{L_c}\,\Psi, \quad (3.18)$$

and use the analytical solution to find

$$\Psi_0 = 2\sqrt{\beta}\coth(2\sqrt{\beta}), \quad \Psi = 2\sqrt{\beta}\,\frac{\cosh(2\sqrt{\beta})-1}{\sinh(2\sqrt{\beta})},$$
$$\Psi_1 = 2\sqrt{\beta}\,[-\sinh(2\sqrt{\beta}) + \cosh(2\sqrt{\beta})\coth(2\sqrt{\beta})], \quad (3.19)$$

where $\Psi = \Psi_0 - \Psi_1$. The finite-difference method predicts the approximate expressions $\Psi_0 \simeq c_A = (2+3\beta)/(2+\beta)$, $\Psi \simeq c_C = 4\beta/(2+\beta)$, and $\Psi_1 \simeq c_B = (2-\beta)/(2+\beta)$. The predictions for the function $\Psi$ representing the rate of extravasation are compared in Fig. 2c. The good agreement for values of $\beta$ roughly less than 0.5 suggests that the finite-difference approximation provides us with good estimates for the rate of fluid escaping through the capillary walls.

It is of interest to examine the rate of extravasation when all physical and geometrical parameters and the end pressures are held fixed, and the length of the capillary tube increases. We note that the parameter $\beta$ is proportional to the square of the tube length, $L_c^2$, and are led to considering the function $\Psi/\sqrt{\beta}$ plotted in Fig. 2d. The results reveal that the finite-difference approximation represented by the dotted line erroneously predicts a maximum. This dichotomy raises a warning flag for the interpretation of the results presented in Sect. 4.

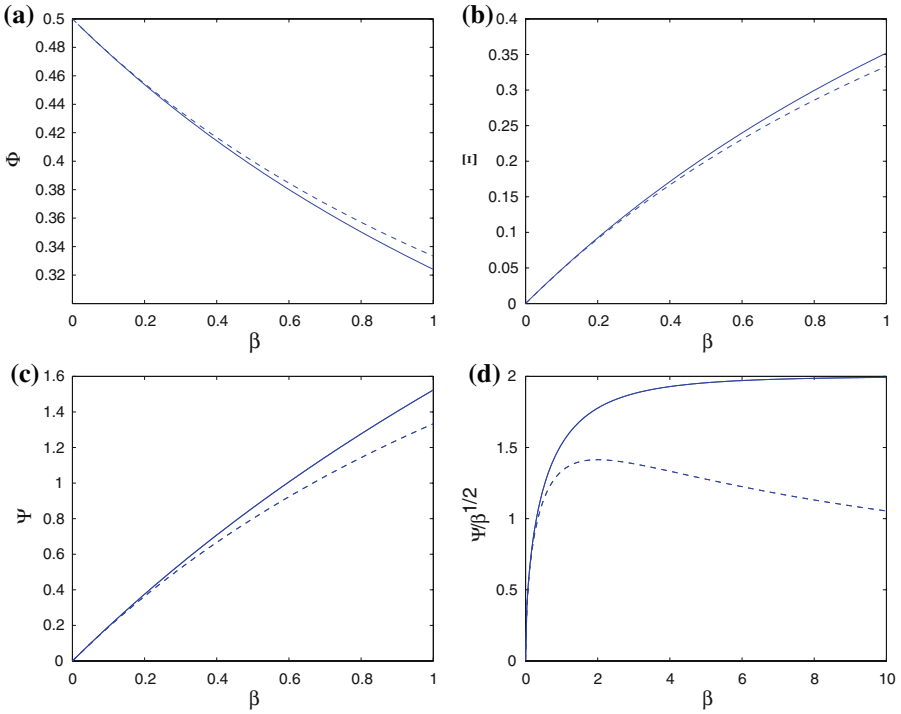


**Fig. 2** Analytical (*solid lines*) and approximate (*dashed lines*) predictions for **a, b** the midpoint pressure in a single capillary tube, **c** the difference in the pressure gradient at the end points representing the rate of extravasation, and **d** the modified difference illustrating the effect of the tube length. The interstitial pressure is assumed to be constant over the outer surface of the capillary

### 3.2 Network nodal pressures

Next, we consider a bifurcation node where one parental capillary segment bifurcates into two segments in three-dimensional space. The local configuration involves four pressure nodes representing network junctions, as shown in Fig. 3. To develop an iterative solution scheme for the computation of the junction pressures, we write a mass balance for the blood flow at the bifurcation node, involving four pressure nodes multiplied by coefficients playing the role of transfer functions, solve for the pressure value at the bifurcation node, and iterate based on the derived expression. The result is the counterpart of the point Gauss-Seidel method (PGS) for solving sparse systems of linear equations. The mass balance requires

$$\left(c_A^{(1)}\, p_0 - c_C^{(1)}\, p^{(1)} - c_B^{(1)}\, P_1\right) \frac{a_1^4}{\mu L_1} + \left(c_A^{(2)}\, p_0 - c_C^{(2)}\, p^{(2)} - c_B^{(2)}\, P_2\right) \frac{a_2^4}{\mu L_2}$$
$$+ \left(c_A^{(3)}\, p_0 - c_C^{(3)}\, p^{(3)} - c_B^{(3)}\, P_3\right) \frac{a_3^4}{\mu L_3} = 0. \tag{3.20}$$

Solving for $p_0$ provides us with an expression that serves as a basis for the iterations.

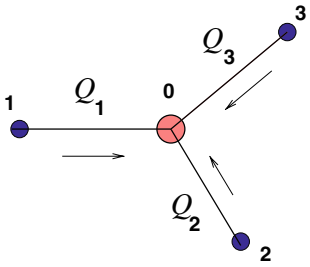


**Fig. 3** Illustration of a capillary bifurcation. A mass balance yields a relation between the pressures at the four segment nodes

### 3.3 Iterative solution

The solution procedure is based on the following algorithm:

1. Generate the vascular geometry in terms of capillary segments, and assign values to the capillary network inlet and outlet capillary pressures, $p_a$ and $p_v$, in lieu of boundary conditions.
2. Make guesses for the nodal capillary segment pressures. In the present numerical simulations, these pressures are set to $p_v$.
3. Make guesses for the interstitial capillary segment pressures. In the numerical simulations, these pressures are set to $p_\infty$.
4. Solve for the pressure at the nodes of the capillary segments by point Gauss-Seidel or SOR iterations pivoted on mass conservation at bifurcations.
5. Update the segment interstitial pressures through the influence matrix arising from the boundary-integral formulation.
6. Return to step 4 and repeat until convergence.

In practice, only a few iterations are necessary for accuracy on the order of $10^{-6}$. When the boundary conditions at the exit points of the network prescribe zero flow rate due to occlusion, the computations correctly predict that all entering fluid perfuses through the tumor, except when $L_p = 0$ where a singular behavior is encountered.

## 4 Results and discussion

A summary of variables and parameters introduced in the theoretical model is shown in Table 1. In this section, we present and discuss results in physical dimensional variables corresponding to the physiological range of conditions. In the numerical simulations, the blood viscosity is set to $\mu = 4.0\,\text{cp} = 4.0 \times 10^{-2}\,\text{g/(cm s)}$, the radius of the inlet capillary segment is set to $a_{c_1} = 6\,\mu\text{m}$, the length of the inlet capillary segment is set to $L_{c_1} = 100\,\mu\text{m}$, and the radius of the outermost capillary segments at the periphery of the network is set to $3.4\mu\text{m}$. The chosen aspect ratio of the capillaries is typical of that encountered in the neoplastic vasculature of solid tumors, which is much smaller than that encountered in normal tissue (e.g., Less et al. (1991)). The linear size of vasculature is comparable to $L \simeq (1-\omega^{m+1})L_{c_1}/(1-\omega)$, where $m$ is the order of the bifurcated tree. The arterial to venous pressure difference is set to $p_a - p_v = 10\,\text{mm}$

**Table 1** Summary of variables and parameters involved in the theoretical model

| | |
|---|---|
| a | Capillary radius |
| $a_{c1}$ | Radius of the first capillary segment |
| $a_{c_{\min}}$ | Radius of the capillary segments at the end of the network |
| $G$ | Green's function |
| $l$ | Arc length along the centerline of a capillary |
| $L_c$ | Length of a capillary segment |
| $L_{c1}$ | Length of the first capillary segment |
| $N_s$ | Number of capillary segments in vascular tree |
| $\mathbf{n}$ | Normal vector |
| $p$ | Tumor pressure |
| $q_e$ | Extravasation flux |
| $p_\infty$ | Ambient tumor pressure |
| $p_c$ | Capillary tube pressure |
| $Q_c$ | Flow rate along a capillary |
| $L_p$ | Vascular permeability |
| $S_V$ | Surface of the vasculature |
| $\beta$ | Dimensionless parameter defined in (3.8) |
| $\epsilon_L$ | Parameter determining the randomness of the capillary segment length |
| $\epsilon_\theta$ | Parameter determining the randomness of the branching angle |
| $\epsilon_z$ | Parameter determining the displacement of a capillary segment off the $xy$ plane |
| $\theta_0$ | Mean branching angle |
| $\kappa$ | Tumor hydraulic permeability |
| $\mu_i$ | Interstitial fluid viscosity |
| $\mu$ | Capillary blood flow viscosity |
| $\Phi$, $\Xi$ | Functions defined in (3.17) |
| $\Psi_0$, $\Psi_1$, $\Psi$ | Functions defined in (3.19) |
| $\omega$ | Contraction ratio of capillary segments at a bifurcation |

Hg, and the tumor surface pressure is set equal to the arterial pressure. Flow rates, capillary and interstitial pressure distributions are then proportional to $p_a - p_v$.

Figure 4a–c illustrates three capillary networks studied with $m = 2$, 4, and 8 branching bifurcations. In all cases, the mean branching semi-angle is $\theta_0 = \pi/10$, and the capillary segment contraction ratio is $\omega = 0.9$. The three random amplitudes determining the capillary tree are set to $\epsilon_L = 0.2$, $\epsilon_\theta = 0.1$, and $\epsilon_z = 0.5$. Of primary interest is the percentage of blood escaping across the vascular walls into the interstitium, termed the fractional leakage and denoted by $\phi$. In the numerical method, the inlet flow rate at the beginning of the entrance segments and the outlet flow rates at the end of each outlet segment are computed from expressions (3.12). The individual outlet flow rates are then summed to give the total outlet flow rate.

Figure 4d–f shows graphs of $\phi$ plotted against the tumor hydraulic permeability $\kappa$ in units of $\text{cm}^4/(\text{dyn s})$ on a log-linear scale. The curves correspond to different values

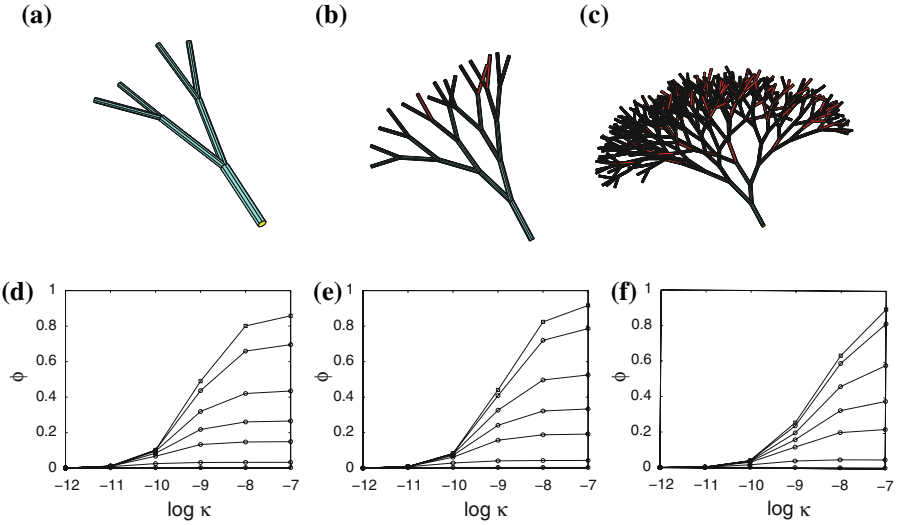


**Fig. 4** **a–c** Capillary networks with $m = 2$, 4, and 8 generations of branching bifurcations. **d–f** Percentage of fluid escaping into the interstitium, $\phi$, plotted against the interstitium hydraulic permeability for vascular permeability $L_p = 10^{-9}$ (lowest line), $10^{-8}$, $5 \times 10^{-8}$, $10^{-7}$, $2 \times 10^{-7}$, $5 \times 10^{-7}$, and $10^{-6}$ (squares) $\mathrm{cm}^3/(\mathrm{dyn\ s})$

of $L_p$, ranging from $L_p = 10^{-9}$ (lowest line) to $10^{-6}$ (squares) $\mathrm{cm}^3/(\mathrm{dyn\ s})$ (e.g., Baish et al. 1997; Baxter and Jain 1989; Sands et al. 1988). The results demonstrate that, as $\kappa$ increases, the fractional leakage $\phi$ tends to a limiting value determined by the value of $L_p$, corresponding to uniform interstitial pressure equal to the ambient pressure, $p_\infty$. Thus, the pressure field developing inside the tumor due to extravasation has a strong effect on the fractional leakage for values of $\kappa$ in the physiological range $10^{-9}$ to $10^{-12}$ $\mathrm{cm}^4/(\mathrm{dyn\ s})$; the lower limit corresponds to normal tissue (e.g., Jain 1987). Increasing the vascular permeability, $L_p$, while holding the tumor hydraulic permeability, $\kappa$, constant causes a monotonic increase in the fractional leakage up to a limit determined by $\kappa$.

The graphs of the fractional leakage presented in Fig. 4d–f for vascular trees of increasing length and complexity show similar qualitative behavior. As the order of the bifurcating network is doubled from 2 to 4 and then to 8, the curves are shifted to the right, and this appears to indicate that, as the geometrical index $m$ increases while $\kappa$ and $L_p$ are kept constant, the fractional leakage monotonically decreases. To precisely illustrate the effect of the order of the vascular tree, in Fig. 5a,b, we plot $\phi$ against $m$ for two sets of parameters corresponding to a moderate and a large fractional leakage. Duplicate computations were carried out to document the extent of scattering due to the partial randomness of the branching vascular tree. The data indicate that $\phi$ reaches a maximum at a particular value of $m$ for both sets of conditions considered. However, in light of the results presented in Fig. 2d for a single straight capillary with a constant interstitial pressure on the outer side, the occurrence of a maximum must be carefully considered. The computations were repeated using the expressions for $\Psi_0$, $\Psi_1$, and $\Psi$ given in (3.19) in place of the coefficients $c_A$, $c_B$, and $c_C$ derived

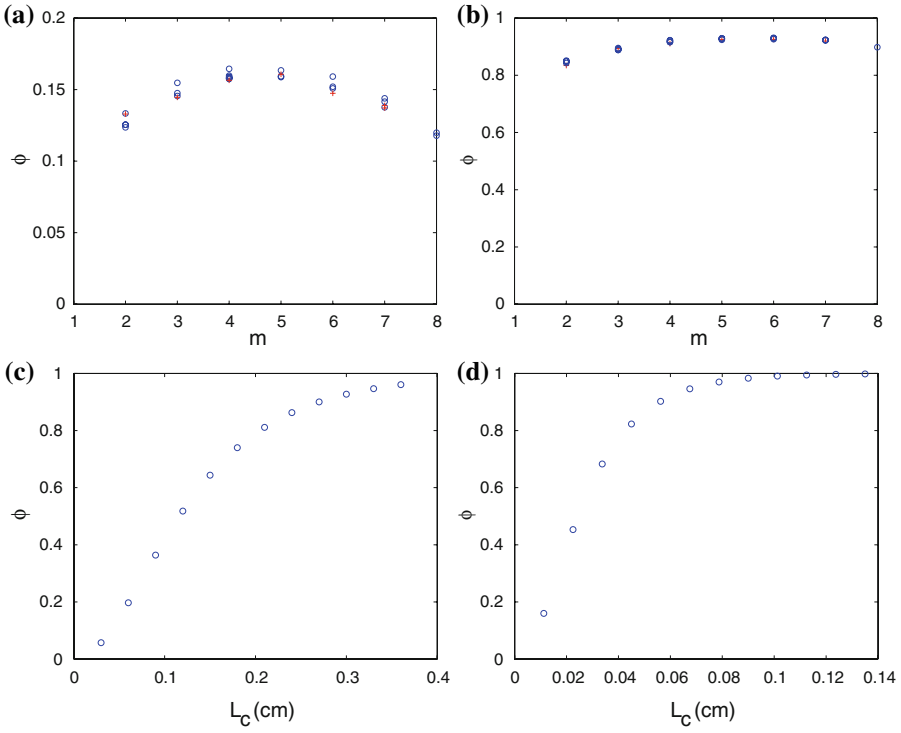


**Fig. 5** **a, b** Dependence of the fractional leakage, $\phi$, on the vasculature order, $m$, for **a** $\kappa = 10^{-9}$ cm$^4$/(dyn s), $L_p = 5 \times 10^{-8}$ cm$^3$/(dyn s), and **b** $\kappa = 10^{-7}$ cm$^4$/(dyn s), $L_p = 10^{-6}$ cm$^3$/(dyn s). Multiple data correspond to duplicate computations. **c, d** Dependence of the fractional leakage on the length of a straight tube for values of $\kappa$ and $L_p$ corresponding to cases **a** and **b**

by the finite-difference approximation. The results displayed with crosses in Fig. 5 corroborate the occurrence of a maximum.

It is of interest to compare the present results for a vascular tree with those of the earlier straight tube model (Pozrikidis and Farrow 2003). Computations were performed for a cylindrical tube of radius $a = a_{c_1} = 6$ μm and varying length, $L_c$. Figure 5c, d shows results for the fractional leakage for values of $\kappa$ and $L_p$ corresponding to the network results shown in Fig. 5a, b. In both cases, as the length of the capillary increases, the fractional leakage increases monotonically and tends to the maximum possible value of unity. A possible explanation for the maxima seen in Fig. 5a, b is then that branching capillary segments above a certain level elevate the interstitium pressure and thereby reduce the extravasation flux.

Figure 6a, b illustrates the capillary and interstitial pressure distributions on the outer side of the capillaries in the most advanced network, $m = 8$, for $\kappa = 10^{-9}$ cm$^4$/(dyn s) and $L_p = 5 \times 10^{-8}$ cm$^3$/(dyn s). Under these conditions, the fractional leakage is $\phi = 0.120$. The graphs confirm that neglecting the developing interstitial pressure field due to extravasation has an important effect on the predicted fractional flow rates. Figure 6c,d shows corresponding results for $\kappa = 10^{-7}$ cm$^4$/(dyn s) and

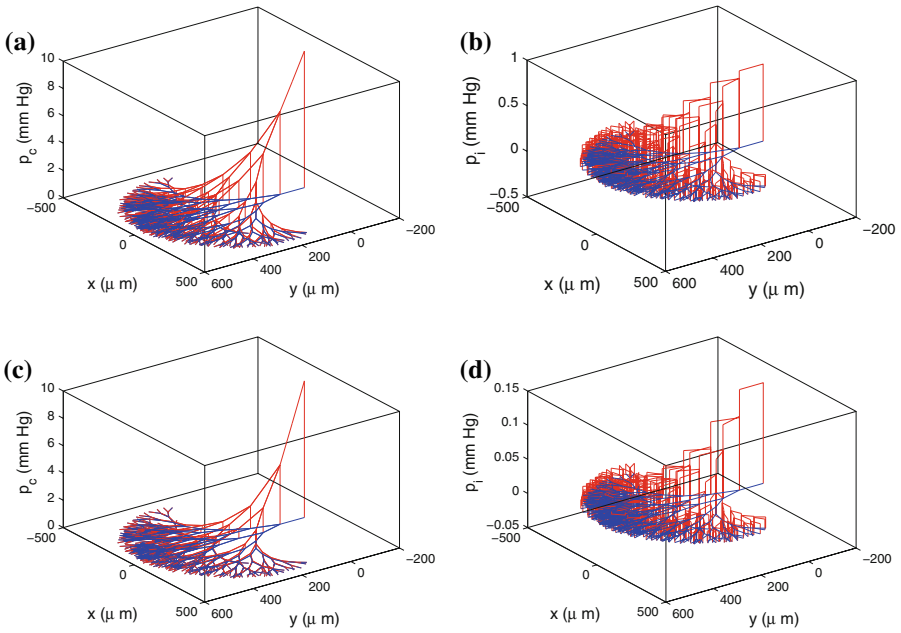


**Fig. 6** **a** Capillary pressure, and **b** interstitial pressure distribution on the outer side of the capillaries in a network with $m = 8$ bifurcations, for $\kappa = 10^{-9}\,\mathrm{cm}^4/(\mathrm{dyn\ s})$ and $L_p = 5 \times 10^{-8}\ \mathrm{cm}^3/(\mathrm{dyn\ s})$. **c, d** Corresponding distributions for $\kappa = 10^{-7}\,\mathrm{cm}^4/(\mathrm{dyn\ s})$ and $L_p = 5 \times 10^{-6}\,\mathrm{cm}^3/(\mathrm{dyn\ s})$

$L_p = 5 \times 10^{-6}\,\mathrm{cm}^3/(\mathrm{dyn\ s})$. Under these conditions, the majority of fluid escapes through the capillary walls, and the fractional leakage is $\phi = 0.898$. The rise in the interstitial pressure is lower than that seen in Fig. 6a,b. Comparison between the graphs shown in Fig. 6 demonstrates that vascular leakage renders the capillary pressure profile upward concave, especially near the entrance point.

The effect of the geometry of the vascular network was further examined by carrying out computations for narrow and widespread vascular networks. Figure 7 illustrates two capillary networks terminating after $m = 8$ bifurcations, one for a large branching angle, $\theta_0 = \pi/4$, and the second for a small branching angle, $\theta_0 = 0.02\pi$. The rest of the geometrical parameters are the same as those corresponding to the results shown in Fig. 4. The graphs of the fractional leakage indicate that the mean branching angle has a noticeable but not profound effect on the extravasation rate.

## 5 Discussion

We have presented an integrated theoretical framework for describing blood flow and fluid motion through the neoplastic vasculature of a solid tumor, with the objective of illustrating the pressure distribution and predicting the extravasation and fractional flux. Computations were performed for a capillary network resembling a branching tree consisting of straight bifurcating capillary segments. The results illustrated the

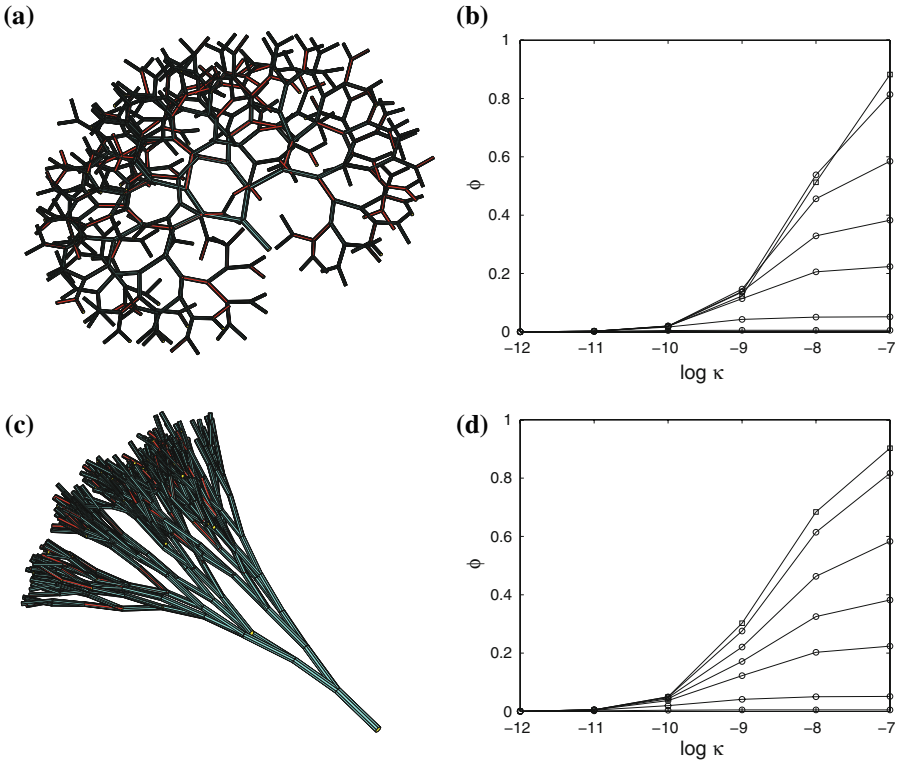


**Fig. 7** Capillary networks terminating after $m = 8$ bifurcations and associated graphs of fractional leakage for mean branching angle **a, b** $\theta_0 = \pi/4$ and **c, d** $0.02\pi$

effect of the interstitium hydraulic and vascular permeability and demonstrated the effect of the length of the capillary tree.

The network structure considered in our simulations exhibits a high degree of geometrical regularity. Although the lengths, branching angles, and elevations of the segments are randomized, the resulting structure is more ordered than that observed in the network structures of tumor and normal tissue. Improved capillary networks with notably disordered geometry and topology can be generated by random walk, invasion percolation, and computational angiogenesis methods (e.g., Tsafnat et al. 2004; Pindera et al. 2008). Flow through these more realistic networks can be handled in a straightforward fashion using the theoretical framework developed in this work, provided that the segment connectivity tables are available.

In an improved model, the straight capillary segments are assigned curved and spiral shapes, and each segment is divided into a number of smaller cylindrical elements interacting through extravasation flow. Segment division into elements improves the error incurred by the assumption of constant interstitial pressure over the outer surface of each segment. The most computationally intensive part of the algorithm is the evaluation of the dense element source and source-dipole hydrodynamic interaction matrices. Direct computation requires $N^2$ floating point operations, where $N$ is on the

order of several thousand or even higher. The high cost of evaluating the surface integrals places a heavy burden on the numerical method and requires the implementation high performance algorithms. The computation of the induced interstitial pressure field can be expedited by the use of adaptive tree code algorithms.

Further extensions and improvements of the theoretical model are possible. First, the pressure dependence of the interstitium permeability can be taken into consideration. Pressure-dependent permeability models of saturated porous media are discussed in the geophysics literature. Because in this case the governing differential equations become nonlinear, the solution must be found by iterative methods built on the computational scheme discussed in this paper, using Kirchhoff's transformation. Second, the dependence of blood viscosity on the capillary radius and discharge hematocrit can be incorporated using published correlations. These extensions will be considered in future work.

**Acknowledgments** This research was supported by a grant provided by the National Science Foundation.

## References

Baish JW, Jain RK (2000) Fractals and cancer. Cancer Res 60:3683–3688

Baish JW, Netti PA, Jain RK (1997) Transmural coupling of fluid flow in microcirculatory network and interstitium in tumors. Microvasc Res 53:128–141

Baxter LT, Jain RK (1989) Transport of fluid and macromolecules in tumors I. Role of interstitial pressure and convection. Microvasc Res 37:77–104

Baxter LT, Jain RK (1990) Transport of fluid and macromolecules in tumors II. Role of heterogeneous perfusion and lymphatics. Microvasc Res 40:246–263

Chaplain MAJ, McDougall SR, Anderson ARA (2006) Mathematical modeling of tumor-induced angiogenesis. Annu Rev Biomed Eng 8:233–257

Chung H-W, Chung H-J (2001) Correspondence re: J. W. Baish and R. K. Jain, Fractals and Cancer. Cancer Res 60:3683–3688 (2000). Cancer Res 61:8347–8351

Dreher MR, Liu W, Michelich CR, Dewhirst MW, Yuan F, Chilkoti A (2006) Tumor vascular permeability, accumulation, and penetration of macromolecular drug carriers. J Nat Cancer Inst 98(5):335–344

El-Kareh AW, Secomb TW (1995) Effect of increasing vascular hydraulic conductivity on delivery of macromolecular drugs to tumor cells. Int J Rad Onc Biol Phys 32:1419–1423

Fleischman GJ, Secomb TW, Gross JF (1986a) Effect of extravascular pressure gradients on capillary fluid exchange. Math Biosc 81:145–164

Fleischman GJ, Secomb TW, Gross JF (1986b) The interaction of extravascular pressure fields and fluid exchange in capillary networks. Math Biosc 82:141–151

Gazit Y, Baish JW, Safabakhsh N, Leunig M, Baxter LT, Jain RK (1997) Fractal characteristics of tumor vascular architecture during tumor growth and regression. Microcirculation 4:395–402

Jain RK (1987) Transport of molecules in the tumor interstitium: a review. Cancer Res 47:3039–3051

Jain RK, Baxter LT (1988) Mechanisms of heterogeneous distribution of monoclonal antibodies and other molecules in tumors: Significance of interstitial pressure. Cancer Res 48:7022–7032

Karshafian R, Burns PN, Henkelman MR (2003) Transit time kinetics in ordered and disordered vascular trees. Phys Med Biol 48:3225–3237

Less JR, Skalak TC, Sevick EM, Jain RK (1991) Microvascular architecture in a mammary carcinoma: branching patterns and vessel dimensions. Cancer Res 51:265–273

Milosevic MF, Fyles AW, Hill RP (1999) The relationship between elevated interstitial fluid pressure and blood flow in tumors: A bioengineering analysis. Int J Rad Oncol Biol Phys 43:1111–1123

Netti PA, Roberge A, Boucher Y, Baxter LT, Jain RK (1996) Effect of transvascular fluid exchange on pressure-flow relationship in tumors: A proposed mechanism for tumor blood flow heterogeneity. Microvasc Res 52:27–46

Pindera MZ, Ding H, Chen Z (2008) Convected element method for simulation of angiogenesis. J Math Biol 57:467–495

Pozrikidis C (1997) Introduction to theoretical and computational fluid dynamics. Oxford University Press, New York

Pozrikidis C (2008) Numerical computation in science and engineering, 2nd edn. Oxford University Press, New York

Pozrikidis C, Farrow DA (2003) A model of fluid flow in solid tumors. Ann Biomed Eng 31:181–194

Sands H, Jones PL, Shah SA, Palme D, Vessella RL, Gallagher BM (1988) Correlation of vascular permeability and blood flow with monoclonal antibody uptake by human clouser and renal cell xenografts. Cancer Res 48:188–193

Sevick EM, Jain RK (1989a) Geometric resistance to blood flow in solid tumors perfused ex vivo: effects of tumor size and perfusion pressure. Cancer Res 49:3506–3512

Sevick EM, Jain RK (1989b) Geometric resistance to blood flow in solid tumors perfused ex vivo: effect of hematocrit on intratumor blood viscosity. Cancer Res 49:3513–3519

Tsafnat N, Tsafnat G, Lambert TD (2004) A three-dimensional fractal model of tumour vasculature. In: Proc. 26th Ann. Int. Conf. IEEE EMBS, pp 683–686

Vaughan ATM, Anderson PW, Dykes P, Chapman CE, Bradwell AR (1987) Limitations to the killing of tumours using radiolabelled antibodies. Br J Radiol 60:567–578

Zhang X-Y, Lick J, Dewhirst MW, Yuan F (2000) Interstitial hydraulic conductivity in a fibrosarcoma. Am J Physiol Heart Circ Physiol 279:H2726–H2734